Vol. 90: 77–94, 2023
https://doi.org/10.3354/cr01718

CLIMATE RESEARCH
Clim Res

Published August 17

Contribution to CR Special 36 'Observed changes in climate over Asia'

Decade-to-decade variations in summer precipitation patterns in eastern China since the 1960s: roles of water vapor transport and sea surface temperature

Pengling Wang[1], Chengyu Song[2], Yanju Liu[1,*], Guowei Yang[1], Jing Wang[3], Chunfeng Duan[4], Yihui Ding[1]

[1]National Climate Centre, China Meteorological Administration, Beijing, 10081, PR China
[2]Heilongjiang Climate Centre, Harbin, 150030, PR China
[3]Tianjin Key Laboratory for Oceanic Meteorology, and Tianjin Institute of Meteorological Science, Tianjin, 300074, PR China
[4]Anhui Climate Centre, Hefei, 230031, PR China

ABSTRACT: Based on the observational precipitation data and multiple reanalysis datasets, this study analyzes the decade-to-decade spatiotemporal evolution of anomalous summer precipitation in eastern China (SPEC) for 1961–2019 and explores the roles of water vapor transport and global sea surface temperatures (SSTs). Results show that SPEC patterns in the last 60 yr were mainly classified into 3 categories: dipole (the 1960s and 1970s), tripole (the 1990s) and quadrupole (the 1980s and 2000s), with marked decade-to-decade variations. In the 2010s, the precipitation pattern exhibited a more complex nature. Obvious differences can be detected in the water vapor channels (WVCs) associated with the 3 SPEC patterns. Specifically, the dipole pattern of the SPEC was mainly related to the Pacific Ocean WVC (POW) and the westerly WVC (WW). The tripole pattern was mainly associated with the Tibetan Plateau Southern Side WVC (TPW), the South China Sea WVC, the POW and the WW. The quadrupole pattern was quite clearly correlated with the Indian Ocean WVC, the Bay of Bengal WVC, the TPW, the POW and the WW. Furthermore, the dipole SPEC pattern was correlated with the Pacific decadal oscillation (PDO), the Indian Ocean basin mode (IOBM) and the Atlantic multi-decadal oscillation. The tripole and quadrupole patterns were related to the IOBM and PDO, respectively. The PDO has a marked influence on the interdecadal shifting of the SPEC pattern in the late 1970s, favoring the formation of the quadrupole SPEC pattern. However, the decadal shifting of the SPEC pattern in the early 1990s is mainly influenced by the IOBM, which favored the formation of the tripole precipitation pattern.

KEY WORDS: Summer precipitation · Spatial distribution pattern · Decade-to-decade variation · Water vapor transport · Sea surface temperature anomaly · Eastern China

1. INTRODUCTION

Eastern China is located in the core area of the East Asian monsoon region, and its summer precipitation (hereafter referred to as SPEC) accounts for nearly 40% of the annual total precipitation. This region is densely populated and economically developed, and the spatiotemporal SPEC patterns can greatly impact regional agricultural production, water resource management, and sustainable economic and social development. Because of this, the multi-timescale variations in SPEC patterns and associated driving

*Corresponding author: liuyanj@cma.gov.cn

Publisher: Inter-Research · www.int-res.com

mechanisms are a particular concern to climatologists (e.g. Ding et al. 2008, Zhang 2015, Zheng et al. 2017, Liu et al. 2020, Li et al. 2022).

Previous studies have shown that the 2 major summer precipitation patterns in the East China monsoon region are the south-to-north meridional tripole and dipole patterns. These 2 patterns exhibit not only interannual variations, but also pronounced interdecadal variations (Huang et al. 2007, Ding et al. 2008, Huang et al. 2011). Specifically, 2 significant interdecadal changes in SPEC patterns occurred in the middle and late 1970s and early 1990s. In the middle and late 1970s, the southerly flow reaching North China in summer weakened markedly, and summer precipitation noticeably decreased in North China and the Yellow River basin, causing severe droughts. In contrast, precipitation in the Yangtze River basin increased dramatically. In the early 1990s, summer precipitation in South China was particularly high (Wu & Wang 2002, Zhou & Huang 2003, Kwon et al. 2007, Ding et al. 2008, Deng et al. 2009). Additionally, these 2 interdecadal changes were characterized by a distinct southward shift of the East Asian summer monsoon rainbands (Ding et al. 2008). Moreover, several studies indicated that the late 1990s also marked the turning point of interdecadal variability in SPEC, i.e. during this period, the summer precipitation increased dramatically in the Yellow and Huaihe River basins but decreased markedly in the Yangtze River basin (Zhu et al. 2011, Huang et al. 2013).

Variation in SPEC is closely related to spatiotemporal variation in water vapor transport over East Asia (Huang et al. 2011, Zhu et al. 2011, Sun & Wang 2015, Chu et al. 2019), and the 2 decadal changes in the precipitation pattern in the middle and late 1970s and early 1990s were both associated with interdecadal variation in water vapor transport in East Asia (X. Z. Li et al. 2012, Sun & Wang 2015). In terms of the spatial distribution of water vapor transport, the interdecadal variability in the tripole and dipole patterns of SPEC is correlated with the summer water vapor transport anomalies over East Asia and the Northwest Pacific, similar to the East Asia/Pacific pattern. Also, such interdecadal variability is closely related to summer water vapor transport anomalies in the mid-high latitude westerlies over Eurasia, similar to the Eurasian teleconnection (Huang et al. 2011).

There are many factors affecting the interdecadal variation in SPEC, such as Eurasian spring snow cover (Zhang et al. 2008, Wu et al. 2009, Cheng et al. 2022), soil moisture (Ding et al. 2009, Lv et al. 2014), atmospheric apparent heat sources over the Tibetan Plateau (Zhang et al. 2019), and sea surface temperature (SST) (Si & Ding 2016, Yang et al. 2017, Zheng et al. 2017, Wang & Li 2019). The influence of SST anomaly patterns is particularly notable. For example, there is an apparent interdecadal shifting of the Pacific decadal oscillation (PDO), which may have caused interdecadal variations in East Asian summer climate in the middle and late 1970s and later, thus affecting the SPEC distribution pattern (Yang & Lau 2004, Deng et al. 2009, Zhu et al. 2011, Si & Ding 2016). Furthermore, the Atlantic multi-decadal oscillation (AMO) is another driving factor of interdecadal variability in summer precipitation in East Asia, which can not only directly influence climate change in East Asia through the teleconnections, but also indirectly modulate the interdecadal variations of the PDO by regulating its phase changes to impact summer precipitation in East Asia (Si & Ding 2016, Sun et al. 2018, Li et al. 2020, Xie & Wang 2020).

Among numerous studies on interdecadal variations in SPEC, the majority focused on the evolution of precipitation at multidecadal timescales or the characteristics of precipitation variation around the turning periods of the precipitation pattern in the 1970s and 1990s (Ding et al. 2008, X. Z. Li et al. 2012, Sun & Wang 2015, Si & Ding 2016, Zhang et al. 2018). However, the evolution characteristics and modulating factors of the SPEC patterns have not been thoroughly investigated at the decade-to-decade timescale. This study aims to systematically reveal the decade-to-decade evolution of the spatial SPEC anomaly pattern in the last 60 yr, especially the characteristics of the phase variation in summertime precipitation since 2000. In light of this, the relationship of decade-to-decade precipitation distribution with water vapor transport and SST variation is further analyzed. This study can deepen the understanding and improve the prediction of SPEC variation at decadal timescales, providing an essential reference for drought/flood prevention and mitigation in the context of of climate change.

The remainder of this paper is organized as follows. Section 2 introduces the data and methods used in this research. Section 3 analyzes the decade-to-decade evolution characteristics of the anomalous SPEC patterns. Section 4 discusses the decade-to-decade variation characteristics of summer water vapor transport over East Asia. Section 5 investigates the correlation of the decade-to-decade SPEC variations with the global basin-scale SST anomalies. The main conclusions and discussion are displayed in Section 6.

2. DATA AND METHODS

2.1. Data

The data used in this research span from 1961 to 2019, including the 0.25° × 0.25° precipitation gridded observation dataset (CN05.1) from the Chinese ground-based meteorological stations developed by the National Climate Center of the China Meteorological Administration. The CN05.1 dataset is based on observations from more than 2,400 ground-based meteorological stations in China and is obtained by superimposing the anomaly fields of each climate variable on its climatic average. The climatic average and anomaly fields of each climate variable are obtained by interpolation, based on the anomaly approach method (Wu & Gao 2013). Currently, the CN05.1 dataset has been widely used in climate change-related studies (Kong & Bi 2016, Li et al. 2019, Wang & Li 2019). In addition, the fifth-generation European Center for Medium-Range Weather Forecasts reanalysis (ERA5) dataset is also used in this study (Hersbach et al. 2020), which includes the monthly surface pressure, wind and specific humidity fields, with 37 vertical levels. The SST data used is monthly global gridded SST reanalysis data, obtained from the National Oceanic and Atmospheric Administration (NOAA) Extended Reconstructed SST version 5 (Huang et al. 2017). The PDO index is calculated based on the first characteristic vector of the empirical orthogonal function (EOF) decomposition of the North Pacific SST anomaly (Mantua & Hare 2002), which can be obtained from the monthly PDO index data derived from the Joint Institute for the Study of the Atmosphere and Ocean (JISAO; http://research.jisao.washington.edu/pdo/). The AMO index is the annual average of the SST anomalies in the Atlantic Ocean of 75°W–7.5°W, 0°–60°N (Enfield et al. 2001), which can be obtained from monthly AMO index data developed by NOAA (https://www.esrl.noaa.gov/psd/data/timeseries/AMO/). The Indian Ocean Basin Mode (IOBM) index is defined as the standardized average of the SST anomalies in the tropical Indian Ocean of 40°E–100°E, 20°S–20°N (Xie et al. 2009).

2.2. Methods

In this study, we deployed a low-pass filter using the 11 yr low-pass filtering to extract the interdecadal component with a 10 yr cutoff period for the filtered variables (Duchon 1979). The climate diagnostic methods, such as the EOF analysis, correlation analysis and regression analysis, are also employed, and the statistical results are tested for significance (Wei 2007). The EOF analysis is mainly used to investigate the main spatial change characteristics of the physical quantity fields, and the significance of their results is tested by the North test (North et al. 1982).

The sliding *t*-test (Wei 2007) is used to test the significance of the interdecadal mutation. For a time series x with a sample size of n, the decadal mutation test is carried out as follows:

First, determine the sample numbers n_1 and n_2 of the 2 subseries x_1 and x_2 before and after the reference point, generally $n_1 = n_2$.

Then, a sliding approach is taken to set the reference points consecutively, and the statistics are calculated sequentially according to Eq. (1). $\overline{x_1}$ and $\overline{x_2}$ indicate the average values of the 2 subseries, and s_1^2 and s_2^2 denote the variances of the 2 subseries. The 2 subseries follow the *t*-distribution with the degrees of freedom $\nu = n_1 + n_2 - 2$. Due to performing the sliding successive calculation, we can obtain a statistic series $t_i (i = 1, 2, \ldots, n - (n_1 + n_2) + 1)$ The statistics are defined as follows (Eq. 1).

$$\begin{cases} t = \dfrac{\overline{x_1} - \overline{x_2}}{s \cdot \sqrt{\dfrac{1}{n_1} + \dfrac{1}{n_2}}} \\ s = \sqrt{\dfrac{n_1 s_1^2 + n_2 s_2^2}{n_1 + n_2 - 2}} \end{cases} \quad (1)$$

The critical value of the significance test is t_α at the significance level of α. If $|t_i| > t_\alpha$, the 2 subseries are determined to have a mutation at this reference point, otherwise the 2 subseries before and after this reference point are regarded not significantly different.

Since we investigate the relationships among the variables on decadal timescales in this study, the effective degrees of freedom (N^{eff}) calculated by Eq. (2) can be used for significance tests on decadal timescales (Pyper & Peterman 1998, Y. Li et al. 2012).

$$\frac{1}{N^{eff}} \approx \frac{1}{N} + \frac{2}{N} \sum_{j=1}^{N} \frac{N-j}{N} \rho_{XX(j)} \rho_{YY(j)} \quad (2)$$

where N denotes the number of samples. $\rho_{XX(j)}$ and $\rho_{YY(j)}$ indicate the autocorrelation coefficients of series X and Y lagging steps, respectively.

The vertical integrations of the water vapor flux (WVT) and its dispersion (WVT_div) are calculated by Eqs. (3) & (4), respectively (Sun & Ding 2008).

$$\mathrm{WVT} = -\frac{1}{g} \int_{P_s}^{300} q \boldsymbol{V} \mathrm{d}p \quad (3)$$

$$\mathrm{WVT\_div} = -\frac{1}{g}\int_{P_s}^{300}\nabla_p\cdot(q\boldsymbol{V})\,\mathrm{d}p \quad (4)$$

where $\nabla_p\cdot(q\boldsymbol{V})$ denotes the horizontal divergence in the pressure coordinate system, g is the acceleration of gravity, P_s is the surface pressure, q is the specific humidity, and $\boldsymbol{V}$ is the horizontal wind vector.

3. DECADE-TO-DECADE EVOLUTION CHARACTERISTICS OF THE SUMMER PRECIPITATION PATTERN IN EASTERN CHINA

3.1. Features of the observed decadal summer precipitation patterns

Fig. 1 shows the decade-to-decade evolution of the spatial distribution of the SPEC anomaly percentage in the past 60 yr (after 11 yr low-pass filtering). The positive precipitation anomalies mainly appeared in the area north of the mainstream of the Yellow River in the 1960s and 1970s. The precipitation anomaly percentage around the Bohai Sea was >20%, while the Yangtze River basin was an area with obviously less precipitation. Thus, the SPEC distribution showed a pattern of flooding in the north and drought in the south. In the 1980s, one positive precipitation anomaly domain was located from Northeast China to the north of North China, and the other was located in the Yangtze River basin. In contrast, the precipitation in the regions of the Yellow and Huaihe River basins and south of the Yangtze River showed pronounced negative anomalies. The overall anomalous SPEC exhibited a quadrupole distribution pattern ('+ − + −') from the north to the south. In the 1990s, the SPEC anomalies showed a tripole pattern ('+ − +'), with the 2 positive precipitation anomaly domains being larger in extent and stronger than in the 1980s. The precipitation north of the Yellow River and the precipitation over Yangtze River and the vast area to the south showed consistent positive anomalies, whereas the precipitation anomalies were negative from the downstream area of the Yellow River to the Huaihe River basin. In the 2000s, the above-mentioned 2 positive precipitation anomaly domains weakened in intensity, narrowed in scope and moved southward. The northern positive precipitation anomaly area moved southward from north of the Yellow River to the Huaihe River basin, while the southern one was mainly located in South China. The vast areas north of the Yellow River and the middle and lower reaches of the Yangtze River were controlled by obvious negative precipitation anomalies. The overall SPEC in the 2000s showed a quadrupole pattern ('− + − +'), roughly opposite to that in the 1980s. In the 2010s, there were 3 positive precipitation anomaly areas, which were located in the northeastern part of northeast China, the central part of North China and the lower reaches of the Yangtze River and some areas to the south. Obviously, the region between Northeast and North China and the Huaihe River basin were the areas with less precipitation. The overall SPEC displays a complex pattern ('+ − + − +') in the 2010s. The above results reveal that the spatial SPEC patterns show marked decade-to-decade variations in the last 60 yr. In addition, there was only one main positive precipitation anomaly area before the 1980s. In the following 30 yr, there were 2 positive precipitation anomaly areas. Meanwhile, the location and range of the positive precipitation anomaly showed marked decade-to-decade differences. Numerous previous studies have demonstrated that the main patterns of the SPEC are dipole and tripole patterns (Huang et al. 2011, Ding et al. 2013, Ren et al. 2016). However, as shown in Fig. 1, the SPEC also exhibited more complex patterns in the 1980s, 2000s and 2010s.

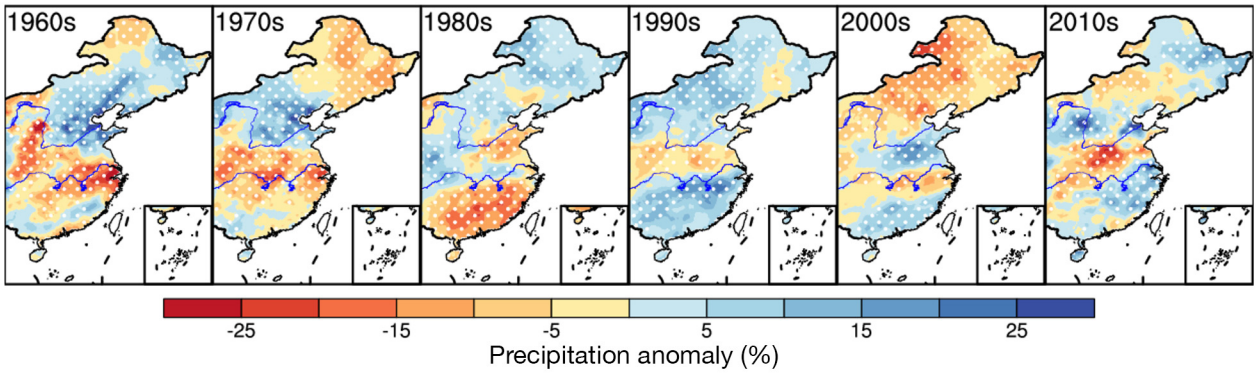

Fig. 1. The decade-to-decade evolution of the spatial distribution of summer precipitation anomaly percentage in eastern China from 1961 to 2019. The values in the dotted areas pass the significance test at the 95% confidence level

3.2. Major modes of the observed decadal summer precipitation patterns

To further understand the spatiotemporal characteristics of the decade-to-decade SPEC patterns, we first perform decadal filtering and then EOF decomposition for the SPEC from 1961 to 2019. Fig. 2 presents the first 4 EOF modes and the corresponding time coefficient series. Their explained variances are 24.3, 19.8, 15.5 and 10.0% (about 70% of the total variance). All 4 patterns pass the North test and are the most significant.

As shown in Fig. 2a, the spatial distribution of the EOF first mode roughly presents a tripole pattern ('− + −'). That is, the precipitation anomalies from the southwest of Northeast China to the north of the Yellow River basin and in the area south of the Yangtze River mainstream show an opposite phase out of those between the Yellow River mainstream and the Yangtze River mainstream. Besides, the spatial pattern of precipitation anomalies is most significant in the area south of the Yangtze River mainstream. The time coefficient series corresponding to the EOF first mode indicates the positive phase in the 1960s and 1980s but the negative phase in the 1990s and middle and late 2010s. In the other periods, the precipitation anomalies are smaller (Fig. 2b). The EOF second mode exhibits a quadrupole pattern ('+ − + −') from Northeast China to South China, i.e. the north of the Yellow River and the middle and lower reaches of the Yangtze River are uniformly positive anomalies in precipitation, while the lower Yellow and Huaihe River basins and South China are uniformly negative anomalies in precipitation (Fig. 2c). The time coefficient series corresponding to the EOF second mode are in a positive phase from the middle 1970s to the middle 1990s and the 2010s and in a negative phase in other periods, with the most significant positive and negative phases in the 1980s and the 2000s, respectively (Fig. 2d). The spatial distribution of the EOF third mode shows a typical north–south antiphase pattern (Fig. 2e), i.e. the phase of precipitation anomalies in the area north of the Yellow River is opposite to that in the Huaihe and Yangtze River basins. The time coefficient series of the EOF third mode is in a negative phase before the late 1970s and in a positive phase in the 1980s and from the late 1990s to the mid-2010s (Fig. 2f). The spatiotemporal distribution characteristics of this mode show a pattern of flooding in the north and drought in the south before 1980 and a pattern of flooding in the south and drought in the north during the 1980s and from the late 1990s to the mid-2010s. In the fourth EOF mode, the phase of precipitation anomalies in North China is opposite to that in most of eastern China, namely more precipitation in North China and less precipitation in Northeast China, from the lower Yellow River to the lower Yangtze River and in the area south of the Yangtze River (Fig. 2g). The time coefficient series of the fourth EOF mode is in a negative phase before the middle 1960s and in the 2010s but in a significant positive phase in the 1970s (Fig. 2h). The spatiotemporal distribution characteristics of the fourth mode indicate that it can explain the phenomena, namely more precipitation in North China and less precipitation in most other areas of eastern China during the 1970s, as well as the opposite spatial distribution of SPEC anomalies between the 2010s and the 1970s.

3.3. Correlation between major modes and the observed decadal summer precipitation patterns

Furthermore, a statistical method of spatial correlation (Chen et al. 2018) is adopted in this research to more objectively reveal the spatial similarity between the spatial distribution of the SPEC decadal evolution and each EOF mode. Table 1 presents the spatial correlation coefficients between the decadal evolution of the SPEC anomaly percentage and the EOF modes. The results show that the spatial distribution of the SPEC in the 1960s is most significantly correlated with the EOF third mode, and the correlation coefficient reaches −0.89, indicating that the SPEC exhibits an obvious characteristic of flooding in the north and drought in the south. Similar to the situation in the 1960s, the spatial distribution of the SPEC in the 1970s is also most significantly correlated with the EOF third mode, and the correlation coefficient is −0.74. However, unlike the 1960s, the correlation between the SPEC spatial distribution and the EOF fourth mode is more obvious, with a correlation coefficient of 0.51, suggesting that the SPEC in the 1970s is characterized by the pattern of flooding in the north and drought in the south and the precipitation in Northeast China is also less. The spatial distribution of the SPEC in the 1980s is significantly correlated with both the EOF first and second modes, and the correlation coefficients are 0.72 (EOF first mode) and 0.78 (EOF second mode). Note that the correlation coefficient with the EOF second mode is the highest. Compared with the distribution characteristics of the EOF first and second modes, the SPEC in the 1980s displays a quadrupole pattern, i.e. more precipitation appears in most areas north of the Yel-

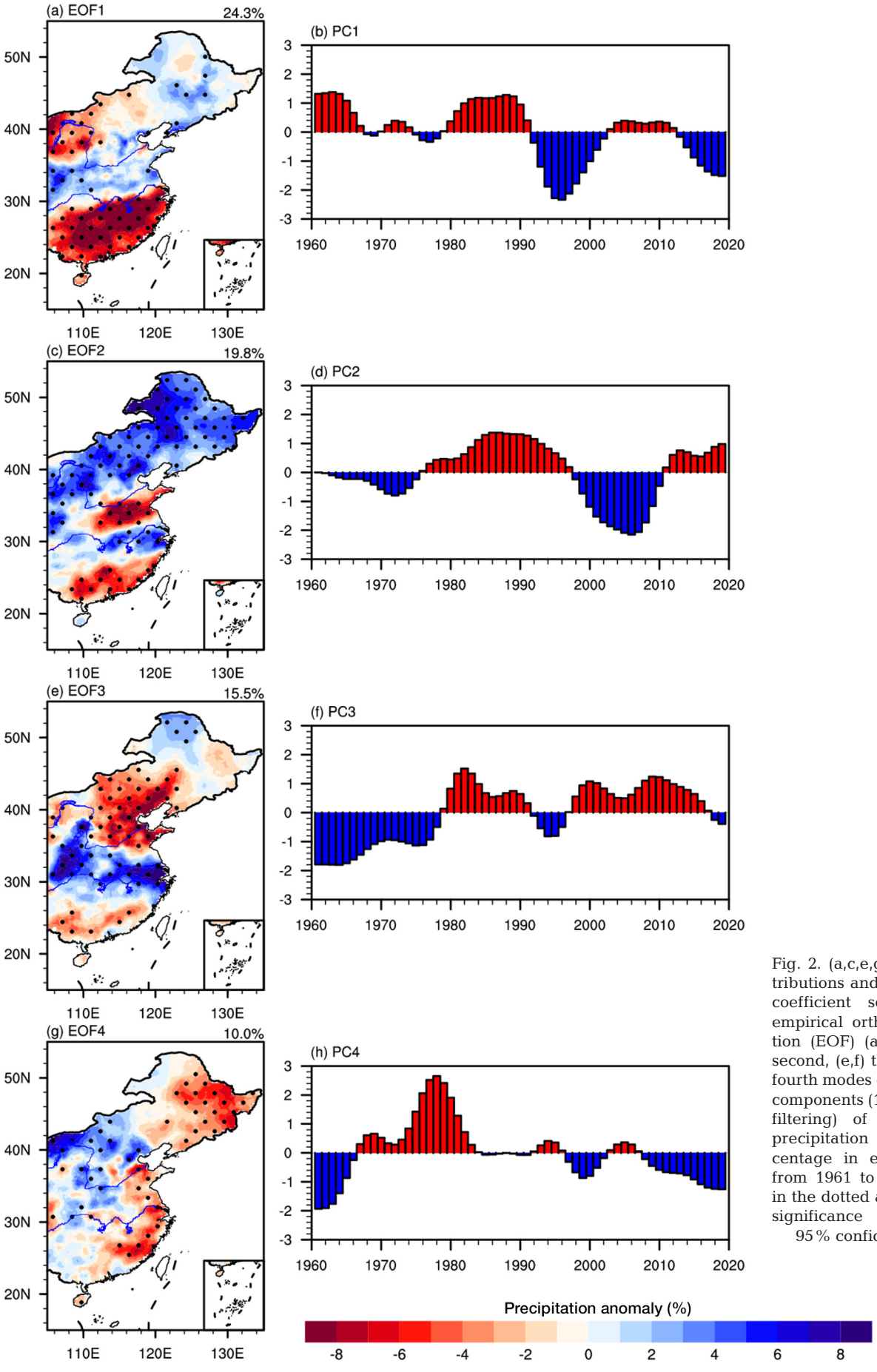

Fig. 2. (a,c,e,g) Spatial distributions and (b,d,f,h) time coefficient series of the empirical orthogonal function (EOF) (a,b) first, (c,d) second, (e,f) third and (g,h) fourth modes of the decadal components (11-yr low-pass filtering) of the summer precipitation anomaly percentage in eastern China from 1961 to 2019. Values in the dotted areas pass the significance test at the 95% confidence level

Table 1. Spatial correlation coefficients between the decade-to-decade anomaly percentage of summer precipitation in Eastern China and the empirical orthogonal function (EOF) modes. Asterisks: correlation coefficients passed the significance test at *90% and **95% confidence levels

	1960s	1970s	1980s	1990s	2000s	2010s
EOF1	0.36*	−0.05	0.72**	−0.68**	−0.23	−0.32
EOF2	0.02	0.01	0.78**	0.27	−0.95**	0.33*
EOF3	−0.89**	−0.74**	0.15	−0.36*	0.07	−0.03
EOF4	−0.17	0.51**	0.21	0.10	−0.10	−0.40*

low River and in the Yangtze River basin, while less precipitation appears in the Yellow and Huaihe River basins and the area south of the Yangtze River. In the 1990s, the spatial distribution of the SPEC is most significantly correlated with the EOF first mode, and the correlation coefficient is −0.68. That is, the SPEC in the 1990s shows a tripole pattern ('+ − +'). In the 2000s, the correlation coefficient between the spatial distribution of SPEC and the EOF second mode reaches −0.95, indicating that the precipitation distribution shows the typical distribution characteristics of quadrupole pattern, i.e. the Yellow and Huaihe River basins and South China receive more precipitation, while north of the Yellow River and the middle and lower reaches of the Yangtze River receive less precipitation. The spatial distribution of SPEC has relatively complex correlations with each EOF spatial mode in the 2010s, and the correlation coefficients with the first, second and fourth modes are −0.32, 0.33 and −0.40, respectively. To qualitatively validate the results of correlations between SPEC and the 4 EOF modes based on EOF analysis, we further conducted the running EOF analysis (Fig. A1 in the Appendix). The results of these 2 analyses are basically identical, namely, the leading EOF is distinct in different decades.

4. CHARACTERISTICS OF DECADE-TO-DECADE VARIATIONS IN SUMMER WATER VAPOR TRANSPORT OVER EAST ASIA

4.1. Decade-to-decade evolution of summer water vapor transport

Regional precipitation is closely related to water vapor transport in the context of the large-scale circulation background. Therefore, in this section, we discuss whether the decadal variations of the SPEC can be reflected by water vapor transport. Fig. 3 shows the decade-to-decade evolutions of summer water vapor transport and its flux divergence anomaly field in East Asia. From the 1960s to 1970s, there was a cyclonic circulation over the southeast of the Mongolian Plateau, while an anticyclonic circulation controlled the vicinity of the Yangtze and Huaihe River basins. Such anomalous circulations resulted in stronger southwest water vapor transport anomalies and water vapor convergence in the Yellow River basin and areas to the north. In addition, the Yangtze River basin was controlled by water vapor divergence, thereby leading to the anomalous precipitation distribution of flooding in the north and drought in the south (Figs. 3a and 3b). Note that in the 1970s, there was a wave train of anticyclonic-cyclonic-anticyclonic-cyclonic-anticyclonic pattern from the north to the south, passing through the northwest and southeast of the Mongolian Plateau, the Yangtze and Huaihe River basins, south of Japan, and east of the Philippine Sea. In the 1980s, the wave train distribution of the anomalous vectors of water vapor transport over the northwest Pacific Ocean changed markedly. Specifically, the cyclonic circulation over the Sea of Okhotsk changed into an anticyclonic circulation, the anticyclonic circulation in the southeast of Japan changed into a cyclonic circulation, and the cyclonic circulation controls the Mongolian Plateau. Northeast China was located at the east side of the cyclonic circulation and the west of the anticyclonic circulation, with stronger southward water vapor transport anomalies and water vapor convergence. South China and the middle and lower reaches of the Yangtze River were located on the south and north sides of the anticyclonic circulation, respectively, whereas South China was controlled by northeast water vapor transport anomalies and water vapor divergence. The southwest water vapor transport anomalies and water vapor convergence existed in the middle and lower reaches of the Yangtze River, while parts of North China were located in the water vapor divergence zone (Fig. 3c). Correspondingly, the SPEC distribution in the 1980s displayed a quadrupole pattern of '+ − + −' from the north to the south, i.e. more precipitation can be found in Northeast China and the middle and lower reaches of the Yangtze River, and the precipitation in North and South China was less (Fig. 1). In the 1990s, the cyclonic circulation anomaly maintained over the Mongolian Plateau. The region north of the Yellow River was located on the southeast side of the cyclone, and this region therefore had southwest water vapor transport anomalies and water vapor convergence. Cyclonic circulation appeared in the west of the area south of the Yangtze River, with a

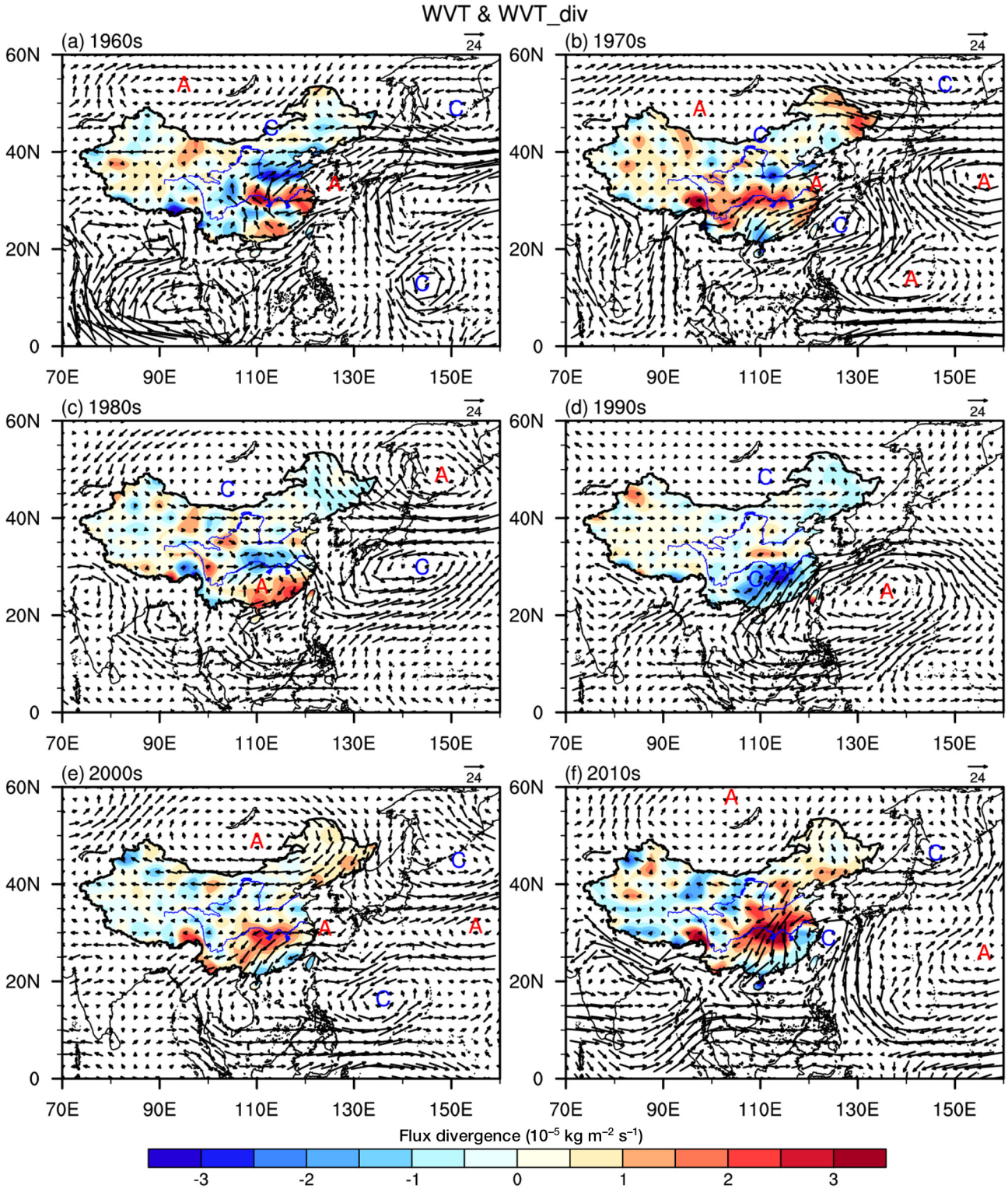

Fig. 3. The decade-to-decade evolution of summer water vapor transport (vector, kg m^{-1} s^{-1}) and its flux divergence (color shading) anomaly fields in East Asia during 1961–2019. 'A' and 'C' denote anticyclonic and cyclonic circulation anomalies, respectively

center located over the northwest of South China. The east of the Yangtze River was controlled by an abnormally strong anticyclonic circulation, whose center was located over the Philippine Sea. We can observe strong southwest water vapor transport anomalies and water vapor convergence in the area south of the Yangtze River. The region between the Yellow River and the Yangtze River was located between the north and south cyclonic circulations. And this region was controlled by pronounced water vapor divergence (Fig. 3d). Correspondingly, the SPEC in the 1990s showed a tripole pattern of '+ − +', i.e. more precipitation appears in the area north of the Yellow River and south of the Yangtze River, and less precipitation appears in the region between the Yellow River and the Yangtze River (Fig. 1). The circulation distribution in the 2000s is roughly opposite to that in the 1980s. The cyclonic circulation over the Mongolian Plateau changes to an anticyclonic circulation, leading to the northeast water vapor transport anomalies in the area north of the Yellow River, accompanied by water vapor divergence, resulting in less precipitation in the region. The anticyclonic circulation center in the area south of Japan was located over the East China Sea, in conjunction with the cyclonic circulation over the low-latitude western Pacific region, resulting in northeast water vapor transport anomalies in the Yangtze River basin, accompanied by water vapor divergence, leading to less precipitation in the region. However, there was water vapor convergence in the Yellow and Huaihe River basins and South China, leading to more precipitation in these areas (Fig. 3e**)**. Thus, the SPEC in the 2000s was characterized by a quadrupole pattern of '− + − +' from the north to the south (Fig. 1). In the 2010s, the anomalous anticyclonic circulation in the Mongolian Plateau and the anomalous cyclonic circulation in the Sea of Okhotsk moved northwestward noticeably. Northeast China changed from being controlled by the anticyclonic circulation to being controlled by a cyclonic circulation, and the precipitation increased in this area. The cyclonic circulation over South China and its east moved northward to the south of the Yangtze River, and its center was located in the East China Sea. This circulation promoted the northward lifting of the southern positive precipitation anomaly area of the SPEC (Fig. 3f). Furthermore, the spatial distribution of the SPEC in the 2010s did not match the corresponding part of water vapor transport and its flux divergence, which is probably due to the complex processes affecting the spatial variation pattern of precipitation in the context of the recent climate warming (Kay 2020).

4.2. Variations in water vapor transport associated with the major precipitation modes

In order to further investigate the connection between the decade-to-decade evolution of the SPEC and the characteristics of summer water vapor transport in East Asia, the time coefficient series corresponding to the first 4 EOF modes of the SPEC from 1961 to 2019 are used to regress onto the water vapor transport and its flux divergence of the whole vertical integration in East Asia during summer. Since the precipitation in periods except the 1980s is negatively correlated with its corresponding typical EOF mode, the negative time coefficient series (−PC1, −PC2, −PC3 and −PC4) corresponding to the first 4 EOF modes are taken for regression analysis to obtain the corresponding spatial distribution of water vapor flux (Fig. 4). Fig. 4a presents the regressed results of water vapor transport and its flux divergence based on the first EOF mode (−PC1). The results indicate that there is a dipole pattern of cyclonic-anticyclonic circulation anomalies over the northwest Pacific Ocean. The northwest-southeast water vapor transport under the anticyclonic–cyclonic–anticyclonic circulation pattern controls the area from the Mongolian Plateau through the middle and lower reaches of the Yangtze River to the Philippine Sea. This distribution of water vapor transport results in stronger southwest water vapor transport and water vapor convergence in the area south of the Yangtze River, and it leads to northeast water vapor transport and water vapor divergence in the area between the Yangtze River and the Yellow River (Fig. 4a). Hence, the precipitation anomalies in the area south of the Yangtze River and between the Yangtze River and the Yellow River are inversely distributed (Fig. 2a**)**. The spatial distributions of the regressed water vapor flux and its divergence corresponding to −PC2 indicate that the summer water vapor transport is characterized by the wave train similar to the East Asia/Pacific pattern from South China through eastern China and southern Japan to the Sea of Okhotsk (Huang et al. 2011). Specifically, there is a cyclonic circulation over South China to the eastern Philippine Sea and an anticyclonic circulation from the area east of the Yangtze River to the subtropical western Pacific Ocean south of Japan. In addition, a cyclonic circulation exists near the Sea of Okhotsk, and a marked anticyclonic circulation controls the Mongolian Plateau (Fig. 4b). This anomalous circulation results in water vapor divergence in Northeast China and the middle and lower reaches of the Yangtze River and water vapor convergence in

the Yellow and Huaihe River basins and South China (Fig. 4b). The SPEC shows a quadrupole pattern of '– + – +' from the north to the south (Fig. 2b). Fig. 4c (–PC3) indicates that the spatial distribution of water vapor transport shows a northwest–southeast type under the anticyclonic–cyclonic–anticyclonic–cyclonic circulation pattern from the northwest and southeast of the Mongolian Plateau through the area east of the Yangtze and Huaihe River basins to the area south of Japan. This results in strong southwest water vapor transport and water vapor convergence in the area north of the Yellow River, and it leads to more pronounced water vapor divergence from the Yellow River to the Yangtze River basin. Therefore, the SPEC presents a spatial pattern of more precipitation in the north and less in the south (Fig. 2c). Regarding the spatial distribution of the regressed water vapor flux and its divergence corresponding to –PC4, there is a cyclonic circulation in the south of the lower reaches of the Yangtze River and an anticyclonic circulation in southern Japan, while Northeast China is controlled by a weak cyclonic circulation. Thus, water vapor convergence appears in the coastal areas of eastern China and southern Japan, and water vapor divergence appears in North China (Fig. 4d). It can be concluded that the areas with more summer precipitation are mainly concentrated in Northeast China and the coastal areas of eastern China (Fig. 2d).

Similar to the results shown in Table 1, because the convergence and divergence of water vapor could be directly related to precipitation anomalies, we quantify the spatial correlations between the first 4 EOF modes of SPEC and the observed decade-to-decade summer water vapor flux divergence anomaly patterns by using the PCs-regressed (corresponding to EOFs of SPEC) water vapor flux divergence fields (Fig. 4) and the observed decade-to-decade summer water vapor flux divergence anomaly fields (Fig. 3). Table 2 presents the spatial correlation coefficients between the decade-to-decade summer water vapor flux divergence anomaly field in eastern China (Fig. 3; shaded areas**)** and water vapor flux divergence regressed onto the negative time coefficient series

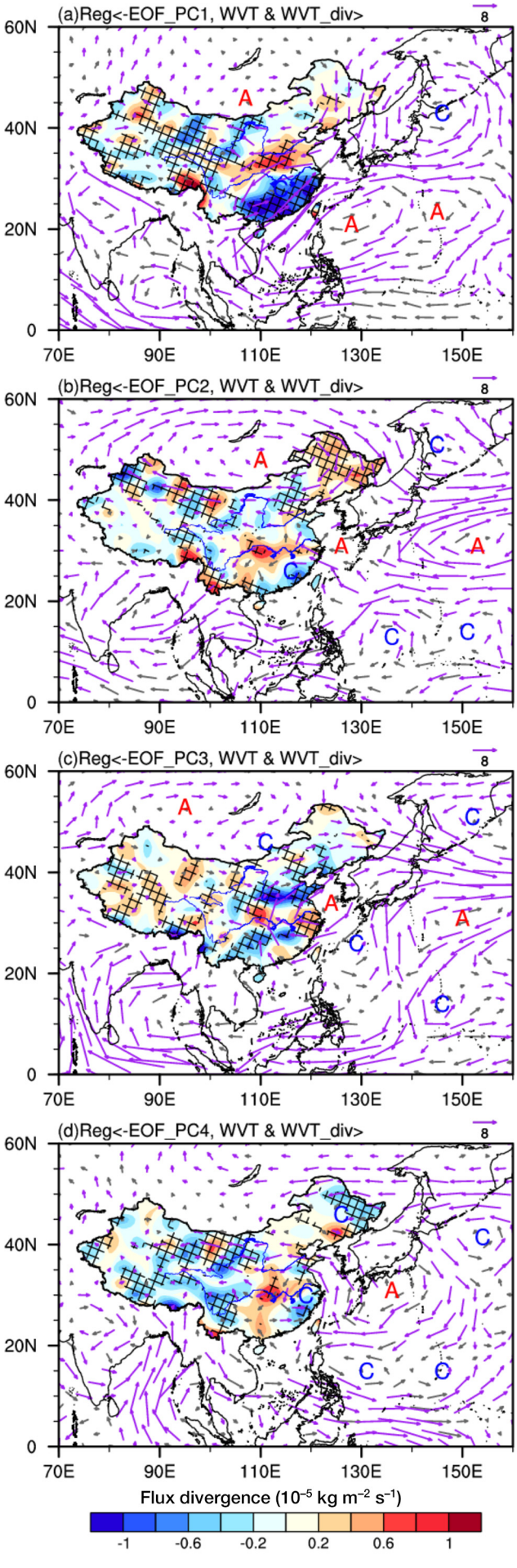

Fig. 4. The summer water vapor transport (vector, kg m^{-1} s^{-1}) and its flux divergence (color shading) regressed onto the negative time coefficient series corresponding to the empirical orthogonal function (EOF) (a) first, (b) second, (c) third and (d) fourth mode of summer precipitation in eastern China during 1961–2019. The values for the purple vectors or in the black crosshatched areas pass the significance test at the 95% confidence level. 'A' and 'C' denote anticyclonic and cyclonic circulation anomalies, respectively

Table 2. The spatial correlation coefficients between the decade-to-decade summer water vapor flux divergence anomaly and water vapor flux divergence anomaly regressed onto the negative time coefficient series (–PCs) associated with the first 4 empirical orthogonal function modes of summer precipitation in Eastern China. Asterisks: correlation coefficients passed the significance test at *90% and **95% confidence levels

	1960s	1970s	1980s	1990s	2000s	2010s
–PC1	–0.39*	–0.02	–0.60**	0.60**	–0.02	0.29
–PC2	0.29	0.26	–0.68**	–0.17	0.82**	0.04
–PC3	0.90**	0.50**	–0.22	0.21	0.03	–0.23
–PC4	0.16	–0.44**	–0.24	–0.08	0.24	0.33*

(–PC1, –PC2, –PC3 and –PC4) corresponding to the first 4 EOF modes of precipitation (Fig. 4; shaded areas**)**. In the 1960s, the spatial correlation coefficient between the summer water vapor flux divergence anomaly field and its –PC3 regression series was the highest (0.90). In the 1970s, the spatial correlation coefficient with the –PC3 regression series was also the highest, while the decadal summer water vapor flux divergence anomaly field showed a sub-correlation with the –PC4 regression series. In the 1980s, the spatial correlation coefficients with both the –PC1 and –PC2 regression series were relatively high, while the highest correlation was with the –PC2 regression series. In the 1990s and 2000s, the water vapor flux divergence anomaly field had the most significant correlation with the –PC1 and –PC2 regression series, while the spatial correlations were complex in the 2010s.

4.3. Relationship between major modes of the SPEC with different water vapor channels

Here we discuss the water vapor channels (WVCs) that affect each distribution pattern of the SPEC. The water vapor for the SPEC in the summer monsoon region mainly originated from the southwest monsoon, subtropical southeast monsoon, cross-equatorial flows and mid-latitude westerlies, and the water vapor transported by these circulations is from the Bengal Bay, thetropical western Pacific, the South China Sea and the North Atlantic Ocean. These 4 WVCs of the Indian monsoon, the South China Sea monsoon, the subtropical monsoon and mid-latitude westerlies basically reflect the comprehensive influence on the summer water vapor transport and climate in China. The westerlies WVC (WW) is much weaker than the 3 low-latitude WVCs (Zhou et al. 2008, Huang & Chen 2010, Yang et al. 2018). According to latitudinal and longitudinal directions, the 4 WVCs are divided into 6 types, namely the Indian Ocean WVC (IOW), the Bay of Bengal WVC (BOBW), the Tibetan Plateau Southern Side WVC (TPW), the South China Sea WVC (SCSW), the Pacific Ocean WVC (POW) and the WW. The IOW intensity can be expressed by the latitudinal flux through the cross-section at 100°E in the range of 10°–20°N (Zhou et al. 2008, Yang et al. 2018). The BOBW intensity can be represented as the longitudinal flux through the cross-section at 20°N in the range of 85°–100°E (Zhou et al. 2008, Yang et al. 2018). The TPW intensity can be indicated as the latitudinal flux through the cross-section at 100°E in the range of 22.5°–27.5°N (Li et al. 2010, Yang et al. 2018). The SCSW intensity can be expressed by the longitudinal flux through the cross-section at 20°N in the range of 110°–120°E (Zhou et al. 2008, Yang et al. 2018). The POW intensity can be represented as the latitudinal flux through the cross-section at 120°E in the range of 25°–30°N (Zhou et al. 2008, Yang et al. 2018). The WW intensity can be indicated as the latitudinal flux through the cross-section at 110°E in the range of 35°–42.5°N (Yang et al. 2018). Previous studies have demonstrated that these 6 water vapor transport channels are closely related to the SPEC (Tian et al. 2002, Zhou et al. 2008, Li et al. 2010, Yang et al. 2018).

Table 3 presents the correlation coefficients of the negative time coefficient series corresponding to the first 4 EOF modes of the SPEC with each WVC index. The tripole precipitation pattern of '+ − +' is positively correlated with the POW and SCSW, but negatively correlated with the TPW and WW, and the most significant positive correlation is with the

Table 3. The correlation coefficients between each water vapor channel index and the negative time coefficient series (–PCs) corresponding to the first 4 empirical orthogonal function modes of the decadal component of summer precipitation in Eastern China. IOW: Indian Ocean water vapor channel; BOBW: Bay of Bengal water vapor channel; TPW: Tibetan Plateau Southern Side water vapor channel; SCSW: South China Sea water vapor channel; POW: Pacific Ocean water vapor channel; WW: westerly water vapor channel. Asterisks: correlation coefficients passed the significance test at *90% and **95% confidence levels

	IOW	BOBW	TPW	SCSW	POW	WW
–PC1	–0.04	0.31	–0.59**	0.88**	0.51**	–0.52**
–PC2	–0.42*	–0.38*	–0.42*	–0.04	–0.40*	–0.56**
–PC3	–0.07	0.20	0.16	0.10	–0.46**	0.37*
–PC4	0.16	0.50**	–0.37*	–0.07	0.07	–0.40*

SCSW. The quadrupole precipitation pattern of '– + – +' shows significant negative correlations with the IOW, BOBW, TPW, POW and WW. The dipole pattern of '+ –' from the north to the south displays a significant negative correlation with the POW and a significant positive correlation with the WW. The negative phase of the EOF fourth mode mainly shows a significant positive correlation with the BOBW and a negative correlation with the TPW and WW.

5. ROLE OF SST ANOMALIES ON DECADE-TO-DECADE VARIATIONS IN SPEC

Here we discuss what external forcing factors may regulate the decade-to-decade variations of the SPEC. The decadal evolution of the summer SST anomalies during 1961–2019 (Fig. 5) indicates that from the 1960s to the 1970s, there were consistent cold SST anomalies in the Indian Ocean, i.e. the negative phase of the IOBM (Xie et al. 2009). The SSTs in the tropical central and eastern Pacific showed significant negative anomalies from the 1960s to the 1970s. Meanwhile, the tropical region with cold SST anomalies extended northward along the west coast of the Americas into the temperate zone of the North Pacific, and the SSTs in the mid-latitude North Pacific showed distinct positive anomalies, similar to the negative phase of the PDO (Mantua & Hare 2002). Compared with the situation in the 1960s, the SST anomalies in the 1970s weakened in the mid-latitude North Pacific, and the cold SST anomalies in the North Atlantic Ocean were stronger and more extensive, namely the negative phase of the AMO (Enfield et al. 2001), as shown in Figs. 5a-b. In the 1980s, the Indian Ocean was controlled by weaker cold SST anomalies. The SST anomalies in the Pacific Ocean changed into the positive phase of the PDO, i.e. the mid-latitude North Pacific is controlled by negative SST anomalies, while its southeastern SST anomalies were positive. In addition, the North Atlantic region exhibited consistent cold SST anomalies in the 1980s (Fig. 5c). Different from the 1980s, the SSTs in parts of the Indian Ocean showed weak positive anomalies in the 1990s, the SST in the tropical central and eastern Pacific increased markedly, and the cold SST anomalies in the northern Pacific weakened (Fig. 5d**)**. In the 2000s, the SSTs in most of the Indian Ocean exhibited positive anomalies, namely the positive phase of the IOBM. The Pacific SST anomalies changed into the negative phase of the PDO, i.e. the range with cold SST anomalies in the tropical central and eastern Pacific extended northward along the west coast of the Americas to the temperate zone of the North Pacific, and the positive SST anomalies prevailed in the mid-latitude North Pacific. In addition, the North Atlantic SST anomalies were consistently positive (Fig. 5e). The spatial distribution of SST anomalies in the 2000s was generally opposite to that in the 1980s. In the 2010s, positive SST anomalies controlled the entire oceanic region except for a few parts in the Pacific and Atlantic Oceans (Fig. 5f).

To reveal the relationship between the SPEC and decadal variations of SSTs in different oceans, the negative time coefficients series corresponding to the 4 modes of EOF of SPEC respectively regressed onto the global SST are shown in Fig. 6. When the SPEC exhibits EOF1 with '+ – +' tripole pattern, the Indian Ocean SST and the North Atlantic Ocean SST show consistent warm anomalies, and the North Pacific Ocean SST shows weak positive PDO-related anomalies (Fig. 6a). When the SPEC exhibits the EOF2 with '– + – +' quadrupole pattern, the Pacific Ocean SST shows significant negative-phase PDO feature, whereas the SST anomalies in the Indian Ocean and North Atlantic Ocean are not obvious (Fig. 6b). When the SPEC exhibits the EOF3 north–south reversed pattern, the Indian Ocean SST and the Atlantic Ocean SST show significant consistent cold anomalies, and the North Pacific SST shows weak negative-phase PDO features (Fig. 6c). When the SPEC exhibits the EOF4 mode, the Pacific Ocean, the North Atlantic Ocean, and central portion of the Indian Ocean regions all show warm SST anomalies (Fig. 6d).

The correlations of the decadal components of the PDO, IOBM and AMO indexes with the negative time coefficient series associated with the first 4 EOF modes are further analyzed, as shown in Table 4. The EOF first mode, i.e. the tripole pattern mainly characterized by more summer precipitation in the area south of the Yangtze River, correlates well with the IOBM, and the correlation coefficient is 0.41, passing the significance test at the 90% confidence level. That is, at the IOBM positive phase, the precipitation is more in the areas north of the Yellow River and south of the Yangtze River and less between the Yellow River and the Yangtze River, and vice versa. The EOF second mode (the quadrupole pattern) is mainly correlated with the PDO, and the correlation coefficient is –0.55, passing the significance test at the 95% confidence level. That is, at the PDO positive phase, the precipitation is more in the area north of the Yellow River and the middle and lower reaches of the Yangtze River and less in the Yellow and Huaihe River basins and South China, and vice versa. The

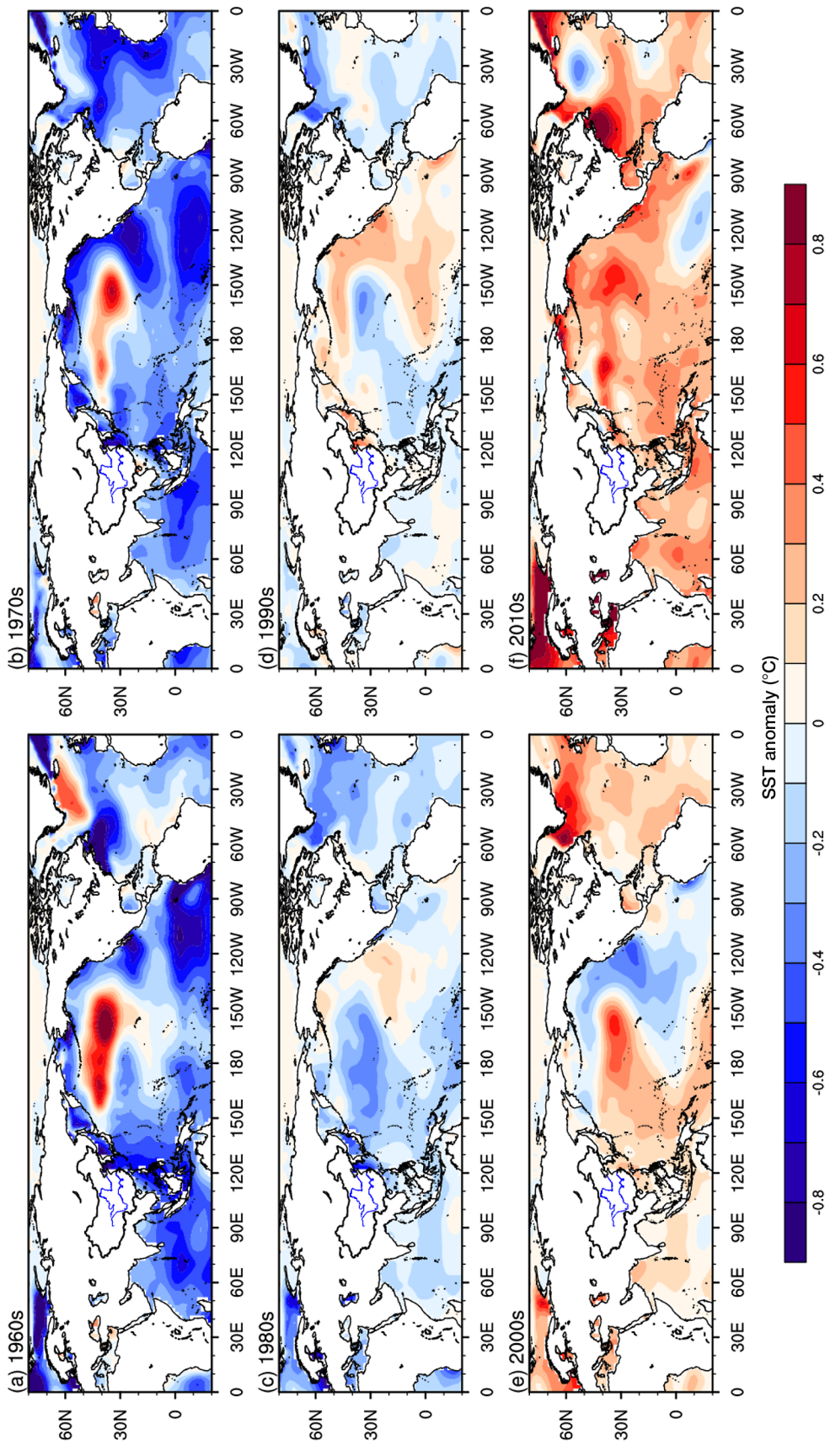

Fig. 5. The evolution of the decade-to-decade summer sea surface temperature (SST) (color shading) anomaly field during 1961–2019

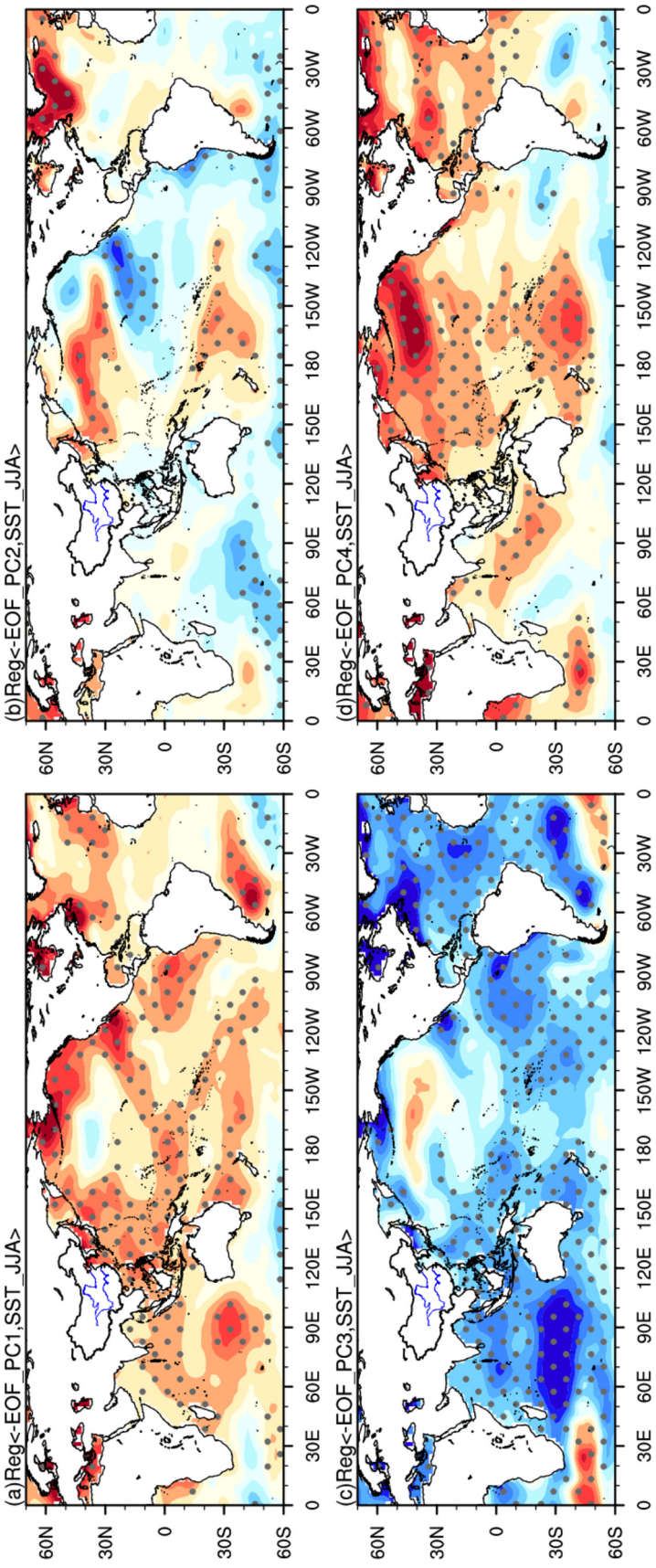

Fig. 6. The summer sea surface temperature (SST) (color shading) regressed on the negative time coefficients series corresponding to the empirical orthogonal function (EOF) (a) first, (b) second, (c) third and (d) fourth mode of summer precipitation in eastern China during 1961–2019. Dotted areas pass the significance test at the 95% confidence level

EOF third mode (north–south anti-phase pattern) has significant correlations with the PDO, IOBM and AMO, and all correlation coefficients pass the significance test at the 90% confidence level. Among them, the correlation is the most significant with the IOBM (–0.70), followed by the AMO (–0.59), and the weakest with the PDO (–0.39). When the PDO, IOBM and AMO are in a positive phase, the SPEC is characterized by a distribution pattern of flooding in the south and drought in the north, and vice versa. All the results of the analyses on the effects of the SST on the second and third EOF precipitation modes are consistent with the findings of Zhang et al. (2018). The EOF fourth mode mainly shows the correlation with the AMO, and the correlation coefficient is 0.52. In summary, the PDO has a marked influence on the decadal shifting of the SPEC pattern in the late 1970s, and the influencing oceanic areas are concentrated in middle latitudes. The spatial distribution of summer precipitation is similar to that of the EOF second mode. This result is also consistent with the findings of previous studies (Qian & Zhou 2014, Wang & Li 2019). However, the decadal shifting of the SPEC pattern in the early 1990s is mainly influenced by the IOBM, and the influencing oceanic areas are concentrated at low latitudes.

6. DISCUSSION AND CONCLUSIONS

In this study, we investigated the decade-to-decade spatiotemporal evolution characteristics of the SPEC patterns from 1961 to

Table 4. The correlation coefficients of the Pacific Decadal Oscillation (PDO), Indian Ocean Basin Mode (IOBM) and Atlantic Multi-decadal Oscillation (AMO) indexes with the negative time series corresponding to the first 4 empirical orthogonal function (EOF) modes of the decadal component of summer precipitation in Eastern China. Asterisks: correlation coefficients passed the significance test at *90% and **95% confidence levels

	−EOF_PC1	−EOF_PC2	−EOF_PC3	−EOF_PC4
PDO	0.30	−0.55**	−0.39*	−0.19
IOBM	0.41*	0.02	−0.70**	0.28
AMO	0.31	0.27	−0.59**	0.52**

2019 based on the CN05.1 precipitation observations, ERA5 reanalysis data and Extended Reconstructed SST data. In addition, we looked at the possible roles of water vapor transport and the global basin-scale SSTs in critical areas on precipitation patterns. The main conclusions are as follows.

The spatial distribution of the SPEC in the last 60 yr showed significant decade-to-decade variations. Before the 1980s, there was a single main positive precipitation anomaly domain. After that, 2 positive precipitation anomaly domains, persisted for 30 yr. The SPEC is mainly classified into 3 patterns: dipole, tripole and quadrupole. The EOF first mode indicates that the SPEC presents a spatial distribution of '− + −' from the north to the south, namely negative anomalies in the areas north of the Yellow River and south of the Yangtze River, and positive anomalies between the Yellow and Yangtze Rivers. The EOF second mode suggests that the SPEC displays a spatial distribution of '+ − + −' from the north to the south, i.e. the precipitation anomalies are all positive in the area north of the Yellow River and the middle and lower reaches of the Yangtze River but negative in the Yellow and Huaihe River basins and South China. The EOF third mode demonstrates that the SPEC shows a spatial distribution of '− +' anti-phase from the north to the south, namely negative anomalies in the area north of the Yellow River and positive anomalies from the area south of the Yellow River to the south of the Yangtze River.

The spatial distribution of the SPEC is closely related to the spatiotemporal variations of summer water vapor transport and its flux divergence over East Asia. When the dipole pattern of cyclonic-anticyclonic circulation dominates over the northwestern Pacific, and the northwest–southeast water vapor transport under the anticyclonic-cyclonic-anticyclonic circulation pattern dominates in the area from the Mongolian Plateau through the middle and lower reaches of the Yangtze River to the Philippine Sea, the SPEC is mainly characterized by a tripolar pattern. The decade-to-decade variations of summer water vapor transport from South China through eastern China and southern Japan to the Sea of Okhotsk are similar to the East Asia/Pacific wavetrain type, and they are associated with the formation of the SPEC quadrupole pattern. The northwest–southeast water vapor transport under the anticyclonic-cyclonic-anticyclonic circulation pattern over the region from the northwest to southeast of the Mongolian Plateau through the east of the Yangtze and Huaihe River basins to southern Japan is related to the SPEC dipole pattern of flooding in the north and drought in the south.

There are noticeable differences in the WVCs associated with the 3 precipitation patterns for the SPEC interdecadal evolution. The dipole precipitation pattern is mainly related to the POW and WW. The tripole pattern is mainly associated with the TPW, SCSW, POW and WW. The quadrupole pattern is more markedly correlated with the IOW, BOBW, TPW, POW and WW.

Analyses of basin-scale SST anomaly patterns indicate that the north–south anti-phase dipole pattern of the SPEC is markedly correlated with the PDO, IOBM and AMO. The tripole precipitation pattern is mainly related to the IOBM, while the quadrupole precipitation pattern is mainly associated with the PDO. In the late 1970s, the PDO had a significant impact on the decadal change of the SPEC pattern, and the influencing oceanic areas were concentrated in middle latitudes. In this period, the spatial distribution of the SPEC is similar to that of the EOF second mode. However, the decadal shifting of the SPEC pattern was mainly influenced by the IOBM in the early 1990s, and the influencing oceanic areas were concentrated at low latitudes. In this period, the spatial distribution of summer precipitation is similar to that of the EOF first mode.

The results of this study indicate that the decade-to-decade evolution of the spatial distribution of summer water vapor transport and its flux divergence in East Asia significantly impact the decadal variation in SPEC. These are mainly regulated by the decadal variation in SST in the Indian, Pacific and Atlantic Oceans. However, the physical mechanisms of how the anomalous SSTs affect the decade-to-decade variations in SPEC spatial distribution needs to be further explored, especially the synergistic effects of the different SST patterns. This research should be conducted through sensitive numerical model experiments. Moreover, global SSTs after the

2010s showed a wide range of consistently positive anomalies. Meanwhile, SPEC since the 2010s also exhibited more complex spatial distribution patterns, which is partially inconsistent with the water vapor flux and its divergence. Therefore, the causes of SPEC spatial distribution since the 2010s needs to be further explored. For example, the combined effects of global warming and natural variability should be considered, and a comprehensive analysis should be carried out on external forcing factors such as sea ice and snow cover.

Acknowledgements: The authors are grateful for the insightful comments of 3 anonymous reviewers. This study is supported by the Major Projects of Basic and Applied Basic Research in Guangdong Province (2020B0301030004), the Second Tibetan Plateau Scientific Expedition and Research Program (2019QZKK0102, 2019QZKK0208), Key Innovation Team of China Meteorological Administration 'Climate Change Detection and Response' (CMA2022ZD03) and Strategic Priority Research Program of the Chinese Academy of Sciences (XDA20100304).

LITERATURE CITED

Chen S, Wu R, Song L, Chen W (2018) Combined influence of the Arctic Oscillation and the Scandinavia pattern on spring surface air temperature variations over Eurasia. J Geophys Res D Atmospheres 123:9410–9429

Cheng F, Li Q, Wang J, Liu YJ, Ding YH, Shen XY, Song CY (2022) Interdecadal variability of spring Eurasian snowmelt and its impact on eastern China summer precipitation. Front Earth Sci 10:927876

Chu Q, Zhi R, Wang Q, Feng G (2019) Roles of moisture sources and transport in precipitation variabilities during boreal summer over East China. Clim Dyn 53:5437–5457

Deng WT, Sun ZB, Zeng G, Ni DH (2009) Interdecadal variation of summer precipitation pattern over eastern China and its relationship with the North Pacific SST (in Chinese). Chin J Atmos Sci 33:835–846

Ding YH, Wang ZY, Sun Y (2008) Inter-decadal variation of the summer precipitation in East China and its association with decreasing Asian summer monsoon. I. Observed evidences. Int J Climatol 28:1139–1161

Ding YH, Sun Y, Wang ZY, Zhu YX, Song YF (2009) Interdecadal variation of the summer precipitation in China and its association with decreasing Asian summer monsoon. II. Possible causes. Int J Climatol 29:1926–1944

Ding YH, Sun Y, Liu YY, Si D and others (2013) Interdecadal and interannual variabilities of the Asian summer monsoon and its projection of future change (in Chinese). Chin J Atmos Sci 37:253–280

Duchon CE (1979) Lanczos filtering in one and two dimensions. J Appl Meteorol Climatol 18:1016–1022

Enfield DB, Mestas-Nuñez AM, Trimble PJ (2001) The Atlantic multidecadal oscillation and its relation to rainfall and river flows in the continental US. Geophys Res Lett 28:2077–2080

Hersbach H, Bell B, Berrisford P, Hirahara S and others (2020) The ERA5 global reanalysis. QJR Meteorol Soc 146:1999–2049

Huang RH, Chen JL (2010) Characteristics of the summer-time water vapor transports over the eastern part of China and those over the western part of China and their difference (in Chinese). Chin J Atmos Sci 34:1035–1045

Huang RH, Chen JL, Huang G (2007) Characteristics and variations of the East Asian monsoon system and its impacts on climate disasters in China. Adv Atmos Sci 24: 993–1023

Huang RH, Chen JL, Liu Y (2011) Interdecadal variation of the leading modes of summertime precipitation anomalies over eastern China and its association with water vapor transport over East Asia (in Chinese). Chin J Atmos Sci 35:589–606

Huang RH, Liu Y, Feng T (2013) Interdecadal change of summer precipitation over Eastern China around the late-1990s and associated circulation anomalies, internal dynamical causes. Chin Sci Bull 58:1339–1349

Huang B, Thorne PW, Banzon VF, Boyer T and others (2017) Extended reconstructed sea surface temperature, version 5 (ERSSTv5): upgrades, validations, and intercomparisons. J Clim 30:8179–8205

Kay JE (2020) Early models successfully predicted global warming. Nature 578:45–46

Kong X, Bi X (2016) Simulation of temperature and precipitation during the last 100 years over southern China by a regional climate model (in Chinese). Clim Environ Res 21:711–724

Kwon M, Jhun JG, Ha KJ (2007) Decadal change in east Asian summer monsoon circulation in the mid-1990s. Geophys Res Lett 34:L21706

Li HX, He SP, Gao YQ, Chen HP, Wang HJ (2020) North Atlantic modulation of interdecadal variations in hot drought events over northeastern China. J Clim 33: 4315–4332

Li JJ, Wang AH, Guo DL, Wang D (2019) Evaluation of extreme temperature indices over China in the NEX-GDDP simulated by high-resolution statistical downscaling models (in Chinese). Acta Meteorol Sin 77:579–593

Li M, Li C, Jiang Z, Zhang X, Zwiers FW (2022) Deciphering China's complex pattern of summer precipitation trends. Earth's Future 10:e2022EF002797

Li XZ, Wen ZP, Zhou W, Wang DX (2012) Atmospheric water vapor transport associated with two decadal rainfall shifts over East China. J Meteorol Soc Japan Ser II 90:587–602

Li YH, Xu HM, Gao YH, Li Q (2010) The characteristics of moisture transport associated with drought/flood in summer over the east of the southwestern China (in Chinese). Acta Meteorol Sin 68:932–943

Li Y, Li JP, Feng J (2012) A teleconnection between the reduction of rainfall in southwest Western Australia and north China. J Clim 25:8444–8461

Liu Y, Ren H, Zhang P, Zuo J, Tian B, Wan J, Li Y (2020) Application of the Hybrid Statistical Downscaling Model in summer precipitation prediction in China (in Chinese). Clim Environ Res 25:163–171

Lv JM, Zhu CW, Ju JH, Lin X (2014) Interdecadal variability in summer precipitation over east China during the past 100 years and its possible causes. Chin J Atmos Sci 38: 782–794 (in Chinese).

Mantua NJ, Hare SR (2002) The Pacific decadal oscillation. J Oceanogr 58:35–44

North GR, Bell TL, Cahalan RF, Moeng FJ (1982) Sampling errors in the estimation of empirical orthogonal functions. Mon Weather Rev 110:699–706

Pyper BJ, Peterman RM (1998) Comparison of methods to

account for autocorrelation in correlation analyses of fish data. Can J Fish Aquat Sci 55:2127–2140

Qian C, Zhou TJ (2014) Multidecadal variability of North China aridity and its relationship to PDO during 1900–2010. J Clim 27:1210–1222

Ren YJ, Song LC, Xiao Y (2016) Interdecadal change of summer precipitation in eastern China during 1880–2010. Daqi Kexue Xuebao 39:445–454 (in Chinese)

Si D, Ding YH (2016) Oceanic forcings of the interdecadal variability in East Asian summer rainfall. J Clim 29: 7633–7649

Sun Y, Ding YH (2008) Effects of intraseasonal oscillation on the anomalous East Asian summer monsoon during 1999. Adv Atmos Sci 25:279–296

Sun B, Wang HJ (2015) Inter-decadal transition of the leading mode of inter-annual variability of summer rainfall in East China and its associated atmospheric water vapor transport. Clim Dyn 44:2703–2722

Sun XQ, Li SL, Sun JL, Hong XW (2018) Differences in intraseasonal activity of Eurasian subtropical zonal wave train and associated Indian summer rainfall in two opposite AMO phases (in Chinese). Chin J Atmos Sci 42: 1067–1080

Tian H, Guo PW, Lu WS (2002) Features of water vapor transfer by summer monsoon and their relations to rainfall anomalies over China. Trans Atmos Sci 25:496–502 (in Chinese)

Wang H, Li DL (2019) The impacts of global sea surface temperature on decadal transitions of summer precipitation over eastern China at global warming transition points. J Trop Meteorol 35:398–408 (in Chinese)

Wei F (2007) Modern climate statistical diagnosis and prediction technology, 2nd edn. China Meteorological Press, Beijing (in Chinese)

Wu J, Gao X (2013) A gridded daily observation dataset over China region and comparison with the other datasets. Chin J Geophys 56:1102–1111 (in Chinese)

Wu RG, Wang B (2002) A contrast of the East Asian summer monsoon–ENSO relationship between 1962–77 and 1978–93. J Clim 15:3266–3279

Wu BY, Yang K, Zhang RH (2009) Eurasian snow cover variability and its association with summer rainfall in China. Adv Atmos Sci 26:31–44

Xie M, Wang C (2020) Decadal variability of the anticyclone in the western North Pacific. J Clim 33:9031–9043

Xie SP, Hu K, Hafner J, Tokinaga H, Du Y, Huang G, Sampe T (2009) Indian Ocean capacitor effect on Indo–western Pacific climate during the summer following El Niño. J Clim 22:730–747

Yang F, Lau KM (2004) Trend and variability of China precipitation in spring and summer: linkage to sea-surface temperatures. Int J Climatol 24:1625–1644

Yang Q, Ma Z, Fan X, Yang ZL, Xu Z, Wu P (2017) Decadal modulation of precipitation patterns over eastern China by sea surface temperature anomalies. J Clim 30: 7017–7033

Yang L, Zhao JH, Feng GL (2018) Characteristics and differences of summertime moisture transport associated with four rainfall patterns over eastern China monsoon region (in Chinese). Chin J Atmos Sci 42:81–95

Zhang R (2015) Changes in East Asian summer monsoon and summer rainfall over eastern China during recent decades. Sci Bull (Beijing) 60:1222–1224

Zhang RH, Wu BY, Zhao P, Han JP (2008) The decadal shift of the summer climate in Eastern China in late 1980s and its possible causes. Acta Meteorol Sin 66:698–706

Zhang Z, Sun X, Yang XQ (2018) Understanding the interdecadal variability of East Asian summer monsoon precipitation: joint influence of three oceanic signals. J Clim 31:5485–5506

Zhang ZH, Cai JJ, Qiao YT, Jian MQ (2019) Interdecadal change in the relation between atmospheric apparent heat sources over Tibetan Plateau and precipitation in Eastern China in summer. Chin J Atmos Sci 43:990–1004 (in Chinese)

Zheng J, Wu MW, Ge QS, Hao Z, Zhang X (2017) Observed, reconstructed, and simulated decadal variability of summer precipitation over eastern China. J Meteorol Res 31: 49–60

Zhou LT, Huang RH (2003) Research on the characteristics of interdecadal variability of summer climate in China and its possible cause. Clim Environ Res 8:274–290 (in Chinese)

Zhou XX, Ding YH, Wang PX (2008) Features of moisture transport associated with the precipitation over North China during July-August. Chin J Atmos Sci 32:345–357 (in Chinese)

Zhu Y, Wang H, Zhou W, Ma J (2011) Recent changes in the summer precipitation pattern in East China and the background circulation. Clim Dyn 36:1463–1473

Appendix.

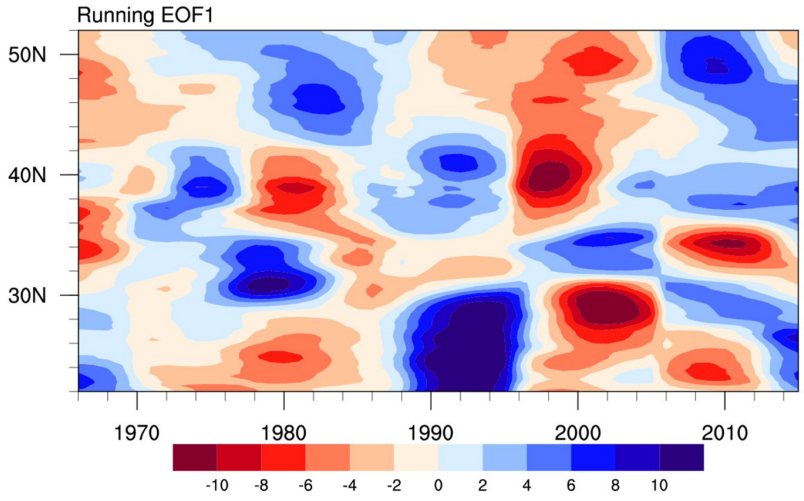

Fig. A1. The time-latitude profile for the 10-yr running empirical orthogonal function (EOF) mode on the zonal (105°–135°E) averaged summer precipitation in eastern China (color shading)

Editorial responsibility: Eduardo Zorita, Geesthacht, Germany
Reviewed by: 3 anonymous referees

Submitted: November 30, 2022
Accepted: June 13, 2023
Proofs received from author(s): August 2, 2023